

RESEARCH ARTICLE

Open Access



HDAC6 activity is a non-oncogene addiction hub for inflammatory breast cancers

Preeti Putchá^{4†}, Jiyang Yu^{2†}, Ruth Rodriguez-Barrueco^{1,8}, Laura Saucedo-Cuevas¹, Patricia Villagrasa⁵, Eva Murga-Penas⁵, Steven N. Quayle⁶, Min Yang⁶, Veronica Castro⁵, David Llobet-Navas¹, Daniel Birnbaum⁹, Pascal Finetti⁹, Wendy A. Woodward⁸, François Bertucci⁹, Mary L. Alpaugh^{7*}, Andrea Califano^{2,3,4*} and Jose Silva^{1*}

Abstract

Introduction: Inflammatory breast cancer (IBC) is the most lethal form of breast cancers with a 5-year survival rate of only 40 %. Despite its lethality, IBC remains poorly understood which has greatly limited its therapeutic management. We thus decided to utilize an integrative functional genomic strategy to identify the Achilles' heel of IBC cells.

Methods: We have pioneered the development of genetic tools as well as experimental and analytical strategies to perform RNAi-based loss-of-function studies at a genome-wide level. Importantly, we and others have demonstrated that these functional screens are able to identify essential functions linked to certain cancer phenotypes. Thus, we decided to use this approach to identify IBC specific sensitivities.

Results: We identified and validated HDAC6 as a functionally necessary gene to maintain IBC cell viability, while being non-essential for other breast cancer subtypes. Importantly, small molecule inhibitors for HDAC6 already exist and are in clinical trials for other tumor types. We thus demonstrated that Ricolinostat (ACY1215), a leading HDAC6 inhibitor, efficiently controls IBC cell proliferation both *in vitro* and *in vivo*. Critically, functional HDAC6 dependency is not associated with genomic alterations at its locus and thus represents a non-oncogene addiction. Despite HDAC6 not being overexpressed, we found that its activity is significantly higher in IBC compared to non-IBC cells, suggesting a possible rationale supporting the observed dependency.

Conclusion: Our finding that IBC cells are sensitive to HDAC6 inhibition provides a foundation to rapidly develop novel, efficient, and well-tolerated targeted therapy strategies for IBC patients.

Introduction

Inflammatory breast cancer (IBC) is the most lethal form of breast cancer (representing approximately 5 % of all breast cancers). Almost all women with primary IBC have lymph node involvement, and at diagnosis approximately

25 % already have distant metastases. Critically, the 5-year survival rate for this disease is only 40 %, compared to an 85 % survival rate in other breast cancer patients [1, 2]. Despite its lethality, IBC remains poorly understood and systemic disease management relies mainly on chemotherapy and standard anti-hormone or anti-human epidermal growth factor receptor-2 (anti-HER2) therapy if the IBC does express these receptors [3, 4].

Due to the unique biology, cancer cell homeostasis presents different dependencies compared to non-transformed cells. Importantly, interfering with these dependencies has been successfully used as a highly selective and low toxicity anticancer strategy [5, 6]. Although efforts are underway to characterize IBC tumors at the molecular level [3, 7, 8] no clinical application has yet

* Correspondence: alpaughm@mskcc.org; califano@c2b2.columbia.edu; jose.silva@mssm.edu

[†]Equal contributors

⁷Department of Surgery, Memorial Sloan Kettering Cancer Center, New York, NY 10065, USA

²Department of Biomedical Informatics, Department of Systems Biology, Center for Computational Biology and Bioinformatics, Herbert Irving Comprehensive Cancer Center, Columbia University, New York, NY 10032, USA

¹Department of Pathology, Icahn School of Medicine at Mount Sinai, New York, NY 10029-6574, USA

Full list of author information is available at the end of the article



emerged from these studies. We thus decided to utilize a comprehensive and unbiased strategy to identify the Achilles heel of IBC cells. We have pioneered the development of genetic tools [9, 10] and experimental [11–13] and analytical strategies [12, 14] to perform RNAi-based loss-of-function studies at a genome-wide level. Importantly, we and others have demonstrated that these functional screens are able to identify essential functions linked to certain cancer phenotypes. Specifically in breast cancer cells, these studies have revealed specific sensitivities associated with luminal and basal subtypes [12, 15] and individual mutated bona fide cancer genes [16, 17]. Thus, we decided to use this approach to identify IBC-specific sensitivities.

Through a genome-wide RNAi screen, we found and validated that the viability of IBC cells depends on histone deacetylase 6 (HDAC6) function. HDAC6 is a class IIb histone deacetylase localizing mainly in the cytosol, where it performs a diverse functional repertoire through deacetylation of multiple targets [18–20]. During the last decade, HDAC6 has emerged as a master regulator of the cellular protective response to cytotoxic accumulation of toxic bioproducts [18–20]. Importantly, there are small molecule inhibitors for HDAC6 currently being tested in advanced clinical trials for other tumor types (myeloma and lymphoid malignancies). Here, using both in vitro assays and in vivo preclinical studies, we demonstrated that Ricolinostat (ACY1215), a leading HDAC6 inhibitor [21], attenuates progression of IBC. These findings provide a direct rationale to developing novel, efficient, and well-tolerated targeted therapies for IBC patients.

Methods

Pooled shRNA screen experimental approach

We performed genome-wide pooled RNAi screens in 13 breast cancer cell lines (Additional file 1, for a table with a complete list and characteristics of the cell lines used). The library pool consists of 58,493 shRNAs integrated into the backbone of miR-30 and cloned into the pGIPZ lentiviral vector (Open Biosystems GIPZ Lentiviral Human shRNA Library). These shRNAs target 18,661 human genes, which account for about 75 % of the human genome. Cell lines were transduced at a multiplicity of infection (MOI) <0.3 in triplicate [12, 13]. After library transduction, cells that have incorporated the GIPZ construct were selected based on the puromycin selection expressed by the library constructs. The surviving cells were allowed to recover for 24 hours. These cells were split into different aliquots containing 70 million cells (approximately 1000 times representation of the library). One aliquot was used for genomic DNA (gDNA) extraction immediately after puromycin selection (t0) and

the other aliquote was passed in culture. Finally, gDNA was extracted again after 10 doubling times (t10).

Next, we utilized NextGen-sequencing via the Illumina HiSeq 2000 at 100 bp resolution to analyze shRNA abundance at t0 and t10 time points [14, 22–24]. As a first step, it is necessary to PCR out the shRNA library integrated in the gDNA of each cell population. For this, PCR-oligos that hybridize in a common region outside the shRNA are used. After this PCR, we obtain a PCR product that contains the shRNA library with the same representation found in the cell population analyzed. The hairpin sequence is extracted from the sequencing read and compared to the reference sequence. Maximum alignment scores are identified as the primary read; if multiple scores exist, the read is marked as ambiguous and not utilized. It is estimated that 75 % of short reads are verifiably read in genome-wide shRNA screens utilizing next generation sequencing (NGS) for deconvolution. An expanded shRNA screen methodology can be found in the supplementary material and methods in Additional file 1).

Pooled shRNA screen analytical approach

Our ultimate goal was to identify genes that selectively compromise IBC cell viability when silenced. This analysis was divided onto several individual steps, as follows.

Individual shRNA analysis

ShRNA reads from T = 0 and T = 10 in all cell lines are first normalized and converted to a log₂ fold-change score (log₂FC), and then fitted to a Gaussian distribution. For each shRNA, individual *t* tests are performed across screen triplicates. Bayesian linear modeling, a type of moderated *t* test, is used to fit the data and accounts for variance generated by the small sample size (*n* = 3) typically utilized in shRNA screens [25]. This method provided us with a fold-change and a statistical *p* value for each shRNA in the library that represents the change in abundance between T = 0 and T = 10 for each individual cell line.

Quality control of the screens

Once a *p* value is obtained for all shRNAs in all cell lines, and in order to further determine the quality of our screen data, we first looked for common essential genes significantly depleted (>=3 cell screened lines, *p* <0.05, 2,555 genes). There is no gold standard set of essential human genes to serve as a benchmark of verifiable screen quality. However, housekeeping genes and genes highly conserved across diverse species have consistently been found to be commonly depleted in shRNA screens, being enriched for essential functions [15, 26]. We used Fisher's exact test to evaluate the

overlap between general essential genes identified by our study and those previously reported [15].

RNAi-based classification of breast cancer cell lines

We determined whether essential genes emerging from these screens could classify breast cancer cell lines. For this, we identified shRNAs significantly depleted ($p < 0.05$) in over one third ($n = 4$) of screened breast cancer cell lines. Then we selected the 30 % that varied most across all of the lines (IQR of z scores over 70 % quartile) and performed unsupervised hierarchical clustering using Pearson correlation and complete linkage clustering.

Selective depletion in IBC cell lines (meta-analysis of shRNA dropout screens)

Since we queried an overall comparison profile between IBCs and non-IBCs, the subsequent p values generated by c method [27] shown in the following formula:

$$Z = \frac{\sum_{i=1}^k z_i}{\sqrt{k}}, z_i \sim N(0, 1)$$

such that each shRNA has two pooled IBC cell line z scores to compare with pooled non-IBC cell line z scores. In the above equation, z_i is the z score indicating the strength of evidence, for example, differential representation score of a gene or a hairpin, in one source, say number i from total number of k sources: z_i follows a standard normal distribution, so the integrated Z score also follows a standard Gaussian distribution assuming independence of all k evidences. The combined two-tailed p value was calculated based on the integrated Z score and utilized such that $p < 0.05$ significance cutoff corresponded to a minimum z comparative score of -1.96 , the negative z score indicating a direction of depletion, positive indicating enrichment. As a further cutoff, we selected shRNAs that had a \log_2FC of at least -1 (depleted by at least 0.5) in both IBC lines compared to non-IBC cell lines.

Functional enrichment of IBC-depleted candidates

In order to see whether IBC-relevant classes of significantly depleted shRNAs are related to functional categories characterizing IBC function and survival, we compared the biological functions of the gene targets (as assessed by gene ontology (GO) categories) of the shRNAs identified from our screen. We used both the Database for Annotation, Visualization, and Integrated Discovery (DAVID) [28], which supports gene annotation functional analysis using Fisher's exact test and gene set enrichment analysis (GSEA) [29], a $K-S$ statistic-based enrichment analysis method, which uses a ranking system, as complementary approaches. For DAVID, the 71 gene candidates selectively depleted in IBC vs. non

IBC cell lines - representing the top best shRNAs - comprised our input list. See also expanded material and methods in Additional file 1.

HDAC6 regulon and HDAC6 score

We used a data-driven approach, utilizing the algorithm for the reconstruction of gene regulatory networks (ARACNe) [30] to reconstruct context-dependent signaling interactomes (against approximately 2,500 signaling proteins) from The Cancer Genome Atlas (TCGA) RNA-Seq gene expression profiles of 840 breast cancer (BRCA [31]), 353 lung adenocarcinoma (LUAD [32]) and 243 colorectal adenocarcinoma (COAD and READ [33]) primary tumor samples, respectively. The parameters of the algorithm were configured as follows: p value threshold $p = 1e - 7$, data processing inequality (DPI) tolerance $\epsilon = 0$, and number of bootstraps (NB) = 100. We used the adaptive partitioning algorithm for mutual information estimation. The HDAC6 sub-network was then extracted and the first neighbors of HDAC6 were considered as a regulon of HDAC6 in each context.

To calculate the HDAC6 score we applied the master regulator inference algorithm to test whether HDAC6 is a master regulator of IBC ($n = 63$) patients in contrast to non-IBC ($n = 132$) samples. For the GSEA method in the master regulator inference algorithm (MARINa), we applied the 'maxmean' statistic to score the enrichment of the gene set and used sample permutation to build the null distribution for statistical significance. To calculate the HDAC6 score we applied the MARINa [34–36] to test whether HDAC6 is a master regulator of IBC ($n = 63$) patients in contrast to non-IBC ($n = 132$) samples. The HDAC6 activity score was calculated by summarizing the gene expression of HDAC6 regulon using the maxmean statistic [37, 38].

Only genes from the BRCA regulon were used when the expression profile data came from HTP-sequencing or Affymetrix array (Fig. 4a and d) but all genes in the list from BRCA, COAD-READ and LUAD regulons were considered when expression data were generated with Agilent arrays (Fig. 4c) due to the low detection of >30 % of the BRCA regulon genes in this platform.

Gene expression microarray data processing

The pre-processed microarray gene expression data (GSE23720, Affymetrix Human Genome U133 Plus 2.0) of 63 IBC and 134 non-IBC patient samples were downloaded from the Gene Expression Omnibus (GEO). We further normalized the data by quantile algorithm and performed non-specific filtering (removing probes with no EntrezGene id, Affymetrix control probes, and non-informative probes by IQR variance filtering with a cutoff of 0.5), to 21,221 probe sets representing 12,624 genes in total. Based on QC, we removed two outlier

non-IBC samples (T60 and 61) for post-differential expression analysis and master regulator analysis.

Cell culture

Cell lines

Non-IBC breast cancer cell lines were all obtained from American Type Culture Collection (ATCC; Manassas, VA 20110 USA). SUM149 and SUM190 were from Asterand, and MDA-MB-IBC3 and Mary-X models were obtained from Drs. Wendy Woodward and Mary Alpaugh, respectively.

Western blots for HDAC6 knockdown

Puromycin-resistant, lentiviral shRNA constructs against HDAC6 or scrambled shRNA (Thermo Scientific GIPZ; Waltham, MA USA 02451) were co-transfected into Phoenix cells along with helper packaging plasmids in order to produce viruses. The jETPEI transfection reagent and protocol was used (Polyplus Transfection). Media were changed at 24 hours. Another 24 hours later, media were collected and filtered through a 0.45- μ syringe unit (BD Falcon). The breast cancer cells of interest were then transduced with the virus and selected for puromycin resistance for 48 hours and allowed to recover for another 48 hours. Protein was harvested to assess knockdown. HDAC6 antibody (rabbit polyclonal, Santa Cruz sc-11420) was used at 1:1000, for 2 hours at room temperature, and β -actin antibody (mouse, monoclonal, BD Biosciences, 558624) was used at 1:5000.

Percentage of apoptotic cells

To measure apoptosis, we utilized the Annexin-V/7-AAD assay BD Bioscience# 559763; San Jose, CA 95131-USA) which detects both early and late events in apoptosis. Floating and attached cells were stained following the kit guidelines to analyze apoptosis and were evaluated using an LSRIIB-FACS analyzer. When used together, 7-AAD and Annexin-V provides a simple staining assay to monitor apoptosis by flow cytometry that allows one to differentiate between 1) intact cells, 2) cells in early apoptosis, which only stain positive for Annexin-V, and 3) cells in later apoptosis, which only stain for 7-AAD.

Cell number

Puromycin-resistant cells transduced with virus expressing shRNAs (against HDAC6 or scrambled control) were first drug selected and then left to recover for 24 hours. Then these cells were plated in 96-well culture plates and the relative number of viable cells was measured in four replicates at different time points using the CellTiter-Glo[®] Luminescent Viability Assay (Promega). The number of cells in each time point was normalized to scrambled shRNA and to the number of cells attached 24 hours after plating.

Drug treatments

For initial testing of Ricolinostat (Acetylon Pharmaceuticals, Inc. Boston, MA USA 02210) and Tubastatin A (Selleck Chemicals; Houston, TX 77054 USA), SUM-149 cells were chosen to test compound efficacy. For in vivo testing, 2-month-old nu/nu female mice were orthotopically transplanted with 1–5 million cells in the right mammary fat pad ($n \geq 6$ were used for each of the treatments). Immunocompromised animals were used to support engraftment of cancer cell lines of human origin. Tumors were monitored until they reached a volume of about 150–200 mm³. At this point, mice were treated with the corresponding inhibitor in dimethyl sulfoxide (DMSO) diluted 1:10 in 5 % dextrose and phosphate-buffered saline (PBS).

Mice were monitored for 24 hours for comparison of Ricolinostat vs. Tubastatin A, and were given a second dose 4 hours before sacrifice. Protein was harvested from tumors for western blot analysis of accumulated α -tubulin levels. All in vitro and in vivo doses were calculated from established doses in the current literature.

For complete treatment response to Ricolinostat, animal tumor cells were inoculated as described above and the animal treated after tumors reached a volume of about 100–200 mm³. Animals were treated with a daily dose of Ricolinostat at 50 mg/kg for 5 days per week during the entire follow up (see treatment schema in Fig. 3c).

Statistical differences were evaluated with the one-tailed *t* test ($n \geq 6$ per cohort). In the corresponding cohorts Paclitaxel was dosed twice per week at 10 mg/kg. All treatments (Ricolinostat, Tubastatin-A and Paclitaxel) were administered intraperitoneally in a final volume of 100 μ l.

Multivariate analysis

In order to evaluate whether the HDAC6 score has any dependence on molecular subtype or clinical subgroups of breast cancer, we fit a multiple regression model of HDAC6 score on IBC and PAM50-defined molecular subtypes (normal, luminal-A, luminal-B, basal, or HER2), IBC and immunohistochemically (IHC)-defined estrogen receptor (ER)–progesterone receptor (PR) status (ER–PR: positive or negative) and IBC, PAM50 and ER–PR and then applied analysis of variance (ANOVA) to compare with the single regression model using IBC only as the predictor.

Ethics, consent and permission

All animal experimentation has been authorized by the IACUC committee at MSSM (Animal Protocol Reference #IACUC-2014-0104). All genetics data analyzed in this manuscript were publically available from The Cancer Genome Atlas (TCGA) and the Molecular Taxonomy of Breast Cancer International Consortium (METABRIC) databases.

Results

Identification of HDAC6 as the Achilles heel of IBC cells

Loss-of-function screening using genetic tools [12, 39, 40] represent a powerful strategy to interrogate gene function at the genome-wide level. We [9, 12] and others [40, 41] have developed RNAi-based genetic approaches to perform high-throughput (HTP) screens in mammalian systems. Using this technology, we performed genome-wide pooled RNAi screens in 13 breast cancer cell lines (2 IBC and 11 non-IBC lines, including 4 luminal, 4 basal-B, 3 basal-A) and 2 non-transformed mammary epithelial lines using a lentiviral library of shRNA-miRs [9] containing approximately 58,000 different shRNAs targeting approximately 18,500 human genes (Fig. 1a). These models were selected because they recapitulate the genetics and drug sensitivity of the main molecular subtypes of human breast cancer [42]. The screens were performed as we have previously described [12, 13] (see also description in “Methods”). The resulting dataset contained data points from 90 independent cell populations.

As a first step in our studies we performed QC studies in our screens. Screens were highly reproducible between biological replicates with correlation between 0.8 and 0.97 for all cell lines (Figure S1a in Additional file 2). Next, we looked for essential genes across multiple cell lines. For this, housekeeping and highly conserved genes are commonly found depleted in shRNA screens, independent of cell type [12, 15, 40, 43]. We thus used these genes as a first metric of screen quality. As previously reported, genes significantly depleted ($p < 0.05$ in $>=3$ screens, 2,555 genes) were significantly enriched in housekeeping functions involving the ribosome, proteasome, spliceosome, DNA replication, protein metabolism and mRNA processing (Figure S1b in Additional file 2). Notably, there was highly significant overlap ($p < 7.2 \times 10^{-18}$; Fisher's exact test) between general essential genes identified by our study and those previously reported [15] (Figure S1c in Additional file 2).

Next, we determined whether essential genes emerging from these screens could classify breast cancer cell lines consistently with functional genomics studies, as we [12] and others [15] have previously shown. As expected, unsupervised hierarchical cluster analysis divided the cell lines into two major groups enriched in luminal and basal subtypes due to subtype-specific sensitivities (Fig. 1b). Interestingly, the IBC cell lines appeared as an independent sub-cluster within the basal-enriched cluster subtype. This suggests that IBC cells present a highly specific profile of essential genes that is not recapitulated by other breast cancer subtypes.

Finally, to achieve an overall profile of IBC vs. non-IBC dependencies, we selected shRNAs significantly and globally depleted in IBC lines vs. non-IBC ($p < 0.05$ and

\log_2FC or $\log_2FC < -1$). Additionally, to prevent selection of genes that were essential in non-transformed cells we required that selected shRNAs were not significantly depleted ($p < 0.05$ and $\log_2FC < -1$) in the two non-transformed lines. This yielded 71 candidate genes (Table S1 in Additional file 3). We show the top 20 as a heatmap, in order of global IBC-specific depletion significance (Fig. 1c).

Next, we investigated whether significantly depleted shRNAs specific to IBC cells cluster within specific functional categories. To create a thorough portrait of functionally enriched IBC pathways, we used both DAVID [28] and GSEA [29] as complementary approaches in order to perform functional enrichment analysis. DAVID analysis, using the 71 candidate genes selectively depleted in IBC vs. non-IBC cells, yielded a set of Gene Ontology (GO) biological processes that were directly and specifically related to one of the candidate genes in the list (i.e., HDAC6) (Fig. 1d). Thus, HDAC6 was the only one of the 71 candidate genes that consistently emerged as part of the top 15 statistically enriched biological processes identified by DAVID. Interestingly, GSEA analysis, including all screened shRNAs ranked by their depletion in IBC vs. non-IBC cells, yielded biological processes that were also specifically related to HDAC6 (Fig. 1d) and HDAC6 was part of 1/3 of the top 15 statistically enriched processes. Thus, both functional enrichment analysis tools provided a comprehensive and intriguing portrait of the role of HDAC6 in IBC survival. Critically, to achieve maximum translational relevance, we paid special attention to candidate targets for which there were clinically relevant pharmacological inhibitors. In this aspect, HDAC6 [18, 20, 44] was also especially interesting, as it represents a druggable target with highly selective inhibitors [21, 45] already available in the clinics, including Ricolinostat [21], which is currently being evaluated in multiple clinical trials (Myeloma NCT01997840, NCT01323751 and NCT02189343 and Lymphoma NCT02091063) as an anticancer drug. Taken together, all of the above provide a strong rationale to select HDAC6 as a primary candidate to validate our screen and further investigate its role in IBC cell survival.

Validation of HDAC6 as a hit in the shRNA screen

Our genome-wide lentiviral shRNA library contains two shRNAs against HDAC6. Thus, in order to individually validate HDAC6 as a screen candidate, we first tested the silencing efficiency of these shRNAs. Lentiviral-mediated individual transduction of both shRNAs in the IBC cell line SUM149 strongly reduced the protein expression of HDAC6 (Fig. 2a). Next, these two shRNAs were used to individually silence the expression of HDAC6 in a series of cell lines consisting of two non-IBC cell lines (MDA-MB-231 and MDA-MB-436)

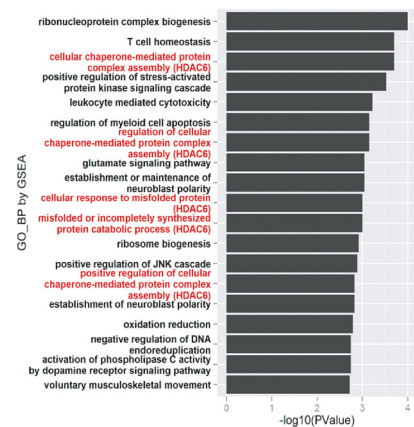
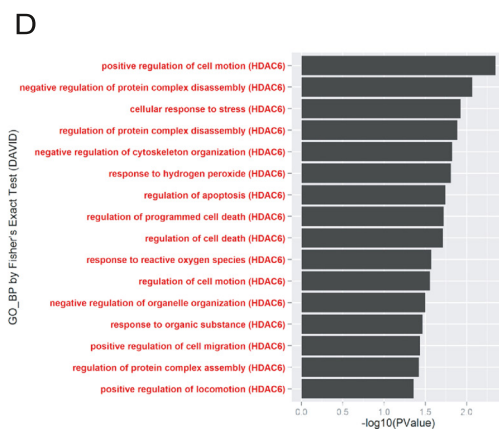
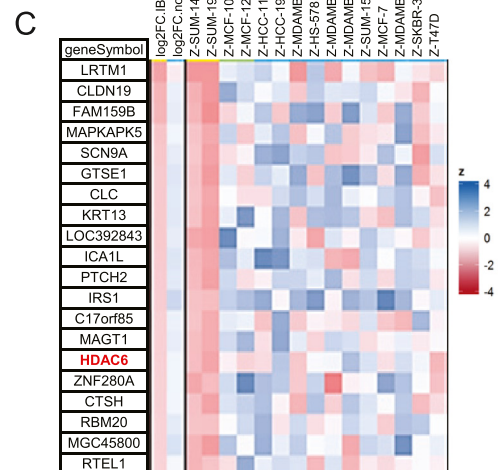
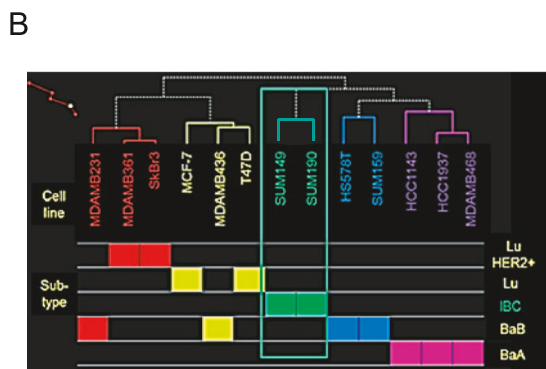
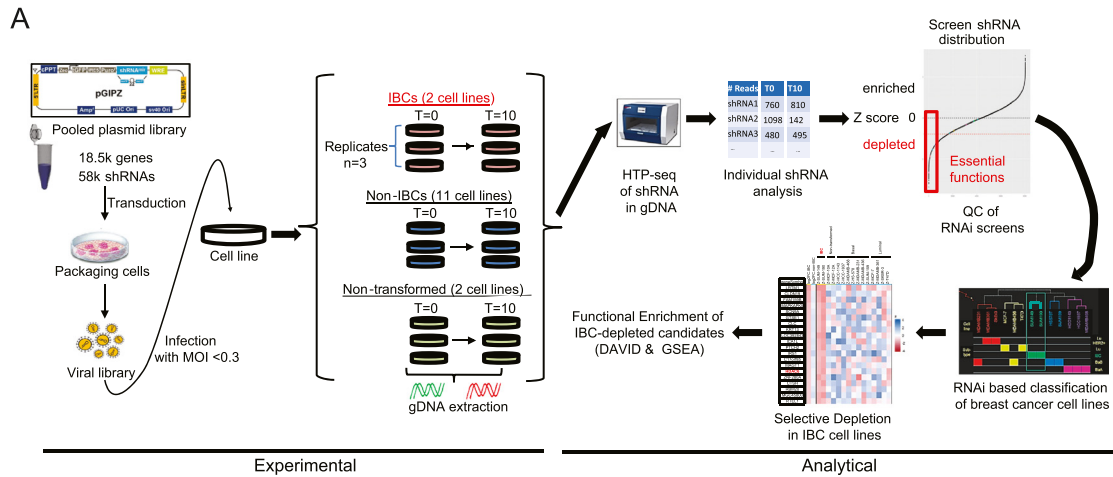


Fig. 1 (See legend on next page.)

(See figure on previous page.)

Fig. 1 Genome-wide loss-of-function screen to identify inflammatory breast cancer (IBC)-specific sensitivities. **a** Graphic representation of the screen strategy described in the text. **b** Unsupervised cluster analysis of shRNA screens functionally classifies breast cancer models based on their molecular subtype. **c** Top 20 genes that specifically compromise the viability of IBC lines when silenced. Heatmap displays the average fold-change in shRNA representation for IBC and non-IBC lines as well as the individual z score for each of the cell lines in the screen. **d** The most statistically significant enriched Gene Ontology (GO) terms (left) and gene set enrichment analysis (GSEA) modules (right) in the 71 genes that specifically compromise the viability of IBC lines when silenced. *HTP* high throughput, *MOI*, multiplicity of infection

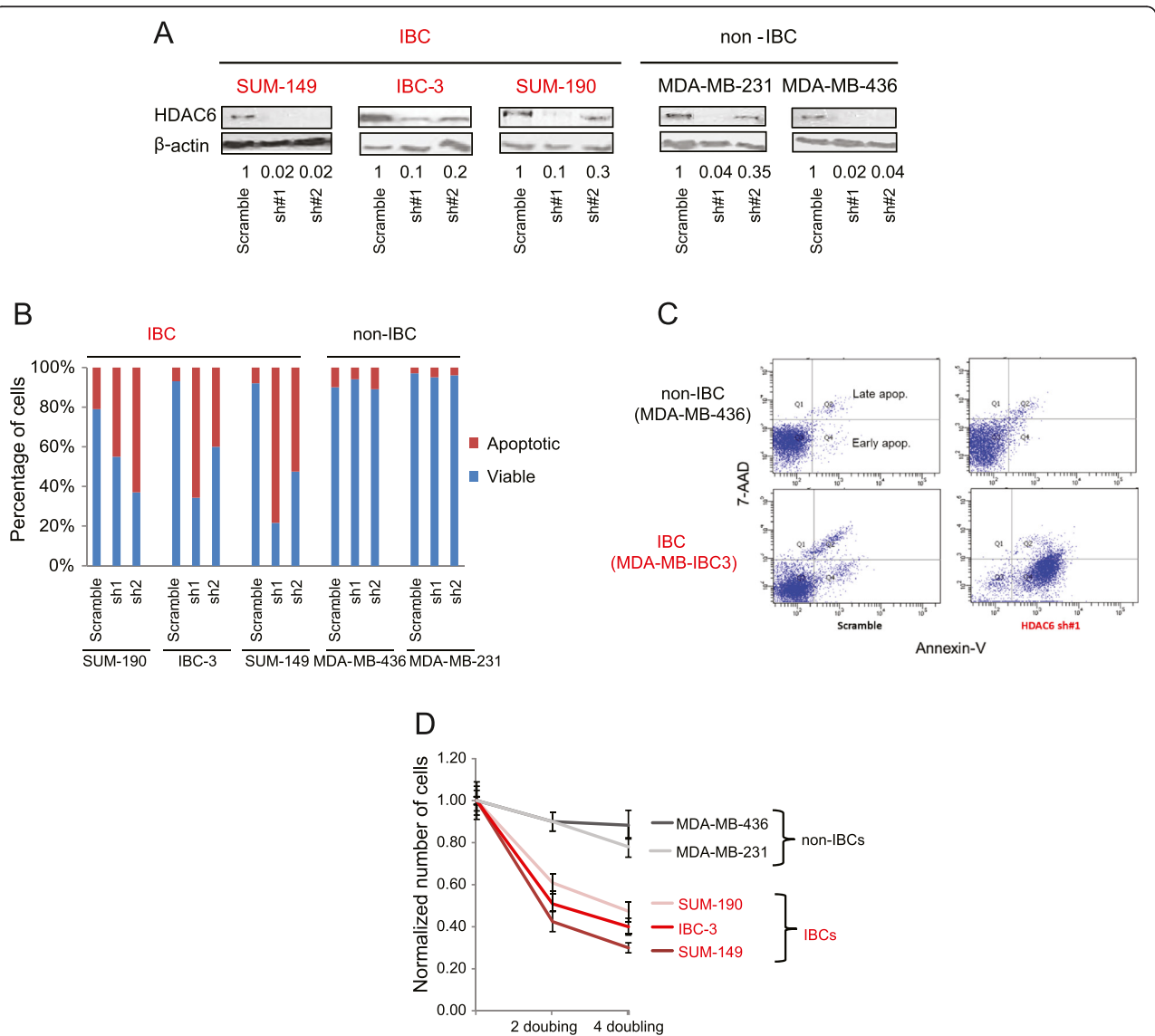


Fig. 2 Validation of histone deacetylase 6 (*HDAC6*) as a positive screen hit. **a** The western blot shows the efficiency of two independent shRNAs in silencing *HDAC6* in different breast cancer cell lines. The numbers below the blots indicate the fraction of protein remained normalized to β -Actin and to the amount detected in cells expressing scrambled shRNA. **b** Graphic representation of Annexin-V/7-AAD assay to measure the induction of apoptosis when *HDAC6* is silenced by the shRNAs shown in **a**. Late apoptosis and early apoptosis are combined. **c** Illustrative example of the FACS data obtained from the Annexin-V/7-AAD assay. **d** Cell numbers after several doubling times in inflammatory breast cancer (IBC) and non-IBC cell lines when *HDAC6* was knocked down (shRNA#1). The data are normalized to the scrambled shRNA control

randomly selected from the cell line series used in the shRNA screens and three IBC cell lines. The IBC cell lines consisted of the two lines used in our screen (SUM149 and SUM190) and a new and independent line, MDA-MD-IBC-3 [46].

We utilized the Annexin V/7-AAD assay to study the induction of apoptosis in each cell line via shRNA knockdown in comparison with control cells transduced with a scrambled shRNA. This assay is able to monitor both early and late events in apoptosis by flow cytometry. These studies revealed that although HDAC6 silencing efficiencies were comparable between IBC and non-IBC models (Fig. 2a), significant apoptotic response was only observed in the IBC lines with minor effects in the non-IBC cells (Fig. 2b and c). As expected, growth curve studies showed reduction of cell proliferation in the IBC cell lines expressing shRNAs targeting HDAC6 compared to controls expressing a scrambled shRNA (Fig. 2d).

Inhibition of HDAC6 compromises the growth of IBC cells in vitro and in vivo

To translate our discovery to preclinical animal models, we decided to evaluate the impact of two of the most potent and specific HDAC6 inhibitors previously described, Tubastatin A [45] and Ricolinostat [21], in the viability of IBC cells. HDAC6 is well known to be responsible for the deacetylation of α -tubulin [44] and accumulation of Ac- α -tubulin is commonly used to evaluate the efficacy of HDAC6 inhibition [18, 20, 21, 44, 45]. Thus, we first compared accumulation of Ac- α -tubulin in SUM149 cells when equal doses of Tubastatin A and Ricolinostat were used. Our results showed that Ricolinostat is a more potent inhibitor of HDAC6 in vitro (Figure S2a in Additional file 4) and in vivo (Figure S2b in Additional file 4).

Next, we evaluated the anticancer activity of Ricolinostat in IBC and non-IBC breast cancer models. For these studies we used three IBC and four non-IBC models [42]. Dose titration curves in cell culture showed that Ricolinostat inhibited the growth of IBC cells more efficiently than non-IBC cells (Fig. 3a). As expected, selective inhibition of cell growth in IBC lines was associated with induction of apoptosis (Fig. 3b). Finally, we performed in vivo preclinical efficacy studies. We used three IBC and two of the non-IBC xenograft models (one luminal and one basal) mentioned above. The IBC cell models included both lines used in our screen (SUM149 and SUM190) and a unique IBC human-patient-derived xenograft (PDX) model (Mary-X) that faithfully recapitulates the dermal lymphatic invasion phenotype characteristic of human IBC [47, 48]. Animals were dosed with 50 mg/kg/day of Ricolinostat, which was previously shown to result in plasma exposure levels

consistent with those observed clinically [21]. As observed in vitro, treatment with Ricolinostat in vivo significantly reduced the growth of IBC models without affecting the non-IBC cells (Fig. 3c). For comparison of the anticancer response we performed parallel treatments with a commonly used chemotherapeutic drug (paclitaxel) (Fig. 3c). Interestingly, in IBC xenograft models Ricolinostat reduced tumor growth at least as much as was observed with paclitaxel treatment.

To further demonstrate that inhibition of HDAC6 compromised the growth of IBC cells we performed cell culture growth studies where SUM149 and MDA-MB-231 were treated with second generation HDAC6 inhibitors that are more selective for HDAC6 than Ricolinostat for off-target inhibition of class-I HDACs. These studies showed that despite efficient inhibition of HDAC6 in both cells lines (as demonstrated by accumulation of acetylated α -tubulin) all these selective HDAC6 inhibitors efficiently reduced the growth of SUM-149 but had a minimal impact on MDA-MB-231 viability (Fig. 3d).

HDAC6 is a master regulator of IBC cells

Next, we aimed to investigate the dependency of HDAC6 in IBCs. We hypothesized that differential expression and/or activity of HDAC6 between IBC and non-IBC cells could mediate IBC cell sensitivity to HDAC6 inhibition. We studied a series of primary breast cancers (63 IBC and 134 non-IBC) representing the largest IBC data series with matched expression and copy number variant (CNV) data from untreated tumors [49]. The HDAC6 locus is located in the chromosome-X at the p11.23 region. This region is rarely amplified in breast cancer, and we found no differences in the mRNA expression level of HDAC6 between IBC and non-IBC samples (Fig. 4d and data not shown). Thus, differential expression of HDAC6 cannot be linked to the different response observed after HDAC6 inhibition in IBC and non-IBC. However, protein activity can be affected by factors such as post-translational modifications, which do not change protein or mRNA levels. We [36, 50, 51] and others [52] have developed methods to infer protein activity in primary cancer samples by reconstructing regulatory networks using mRNA expression profiles. Thus, we used the gene expression profile signatures in over 900 breast cancer samples available in the TCGA BRCA dataset to reconstruct the genome-wide regulatory networks of breast cancer cells, using the ARACNe [30, 36] algorithm. These methods identified a regulon consisting of 162 transcripts as a set of transcriptional targets whose expression is affected by HDAC6 activity (Fig. 4a). GO term enrichment analysis (DAVID) confirmed that this list was enriched in genes involved in canonical HDAC6 functions, such as response to

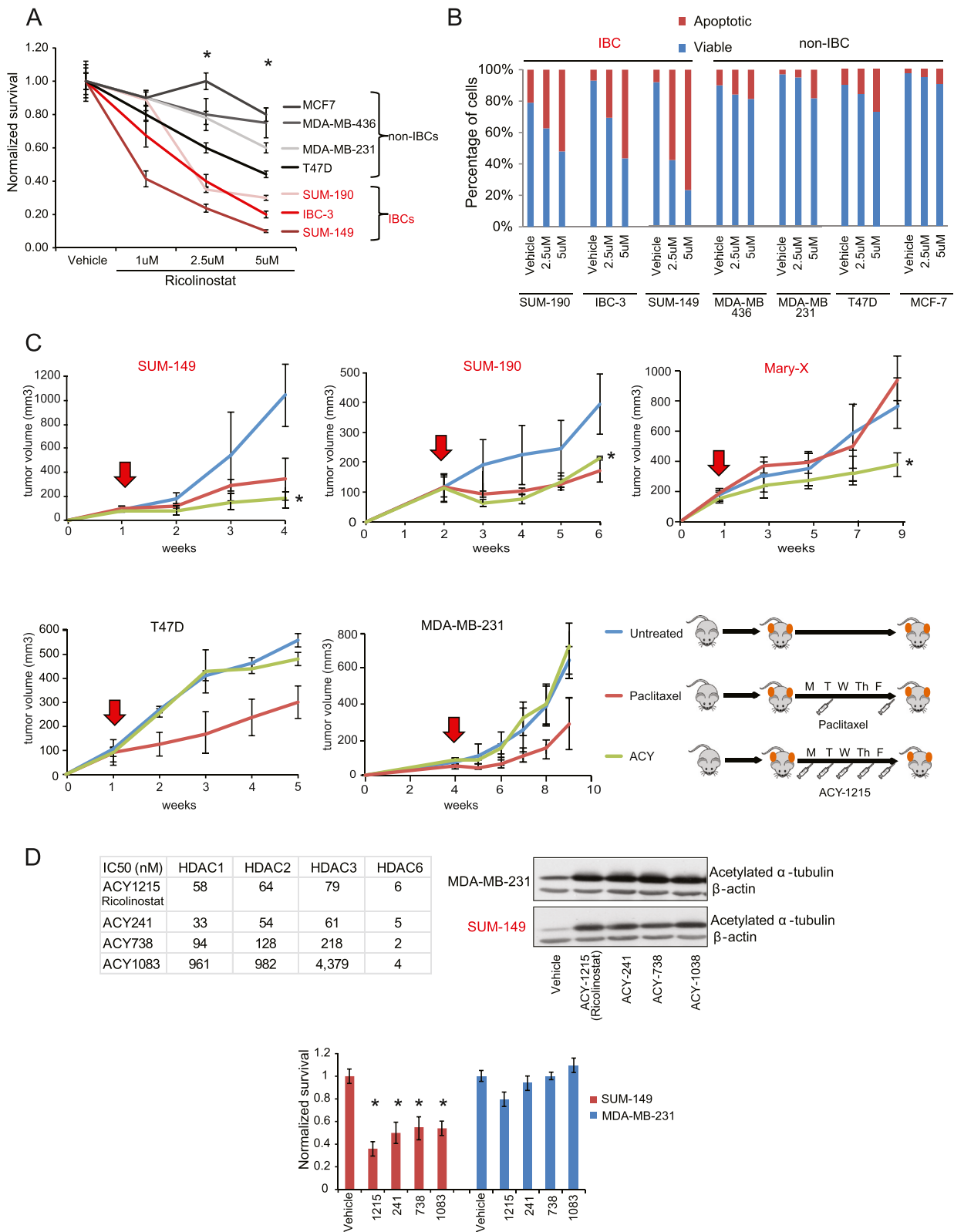


Fig. 3 (See legend on next page.)

(See figure on previous page.)

Fig. 3 Small molecule inhibitors of histone deacetylase 6 (HDAC6) as anticancer strategy in inflammatory (IBC). **a** Normalized numbers of cells when cultures are treated with different concentrations of Ricolinostat for two doubling times. **b** Induction of apoptosis as measured by Annexin-V/7-AAD assay in cells shown in **a**. **c** Growth of IBC cells grown as xenograft models treated with Ricolinostat (50 mg/kg once daily for five days a week). Treating with paclitaxel (10 mg/kg/ twice a week) was also included for comparison of the anticancer response. The treatment regimen is graphically shown. *Red arrows* in each growth curve represent the initiation of the treatments. **d** Biochemical selectivity profiles of the second generation HDAC6 inhibitors (*left table*), their efficacy to induce accumulation of Ac- α -tubulin when IBC and non-IBC cells were treated at 2.5 μ M for 16 hours (*left panel*), and as the impact that treating those cells for one doubling time had on cell number. In all panels *asterisks* indicate statistically significant differences (*t* test, $p < 0.05$) for treatments based on HDAC6 inhibitors: $n >= 6$ for both in vitro and in vivo treatments

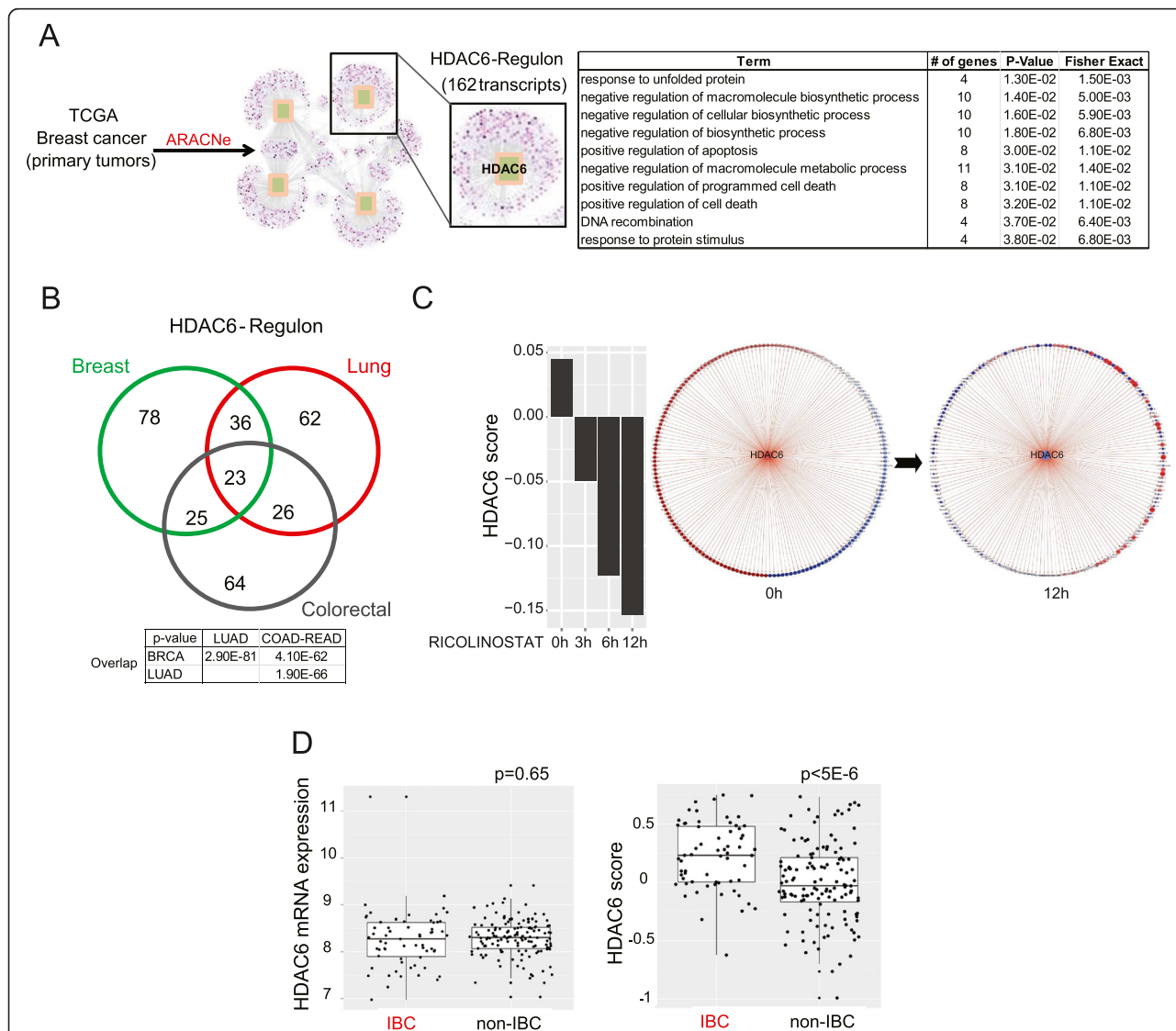


Fig. 4 Histone deacetylase 6 (*HDAC6*) activity is higher in primary inflammatory breast cancer (IBC) than in non-IBC. **a** Identification of the regulon controlled by HDAC6. The table shows the GO terms associated with the 162 transcripts of the HDAC6 regulon in breast cancer. **b** Venn diagrams showing the overlap between the HDAC6 regulons obtained from the analysis of the breast cancer (*BRCA*), colorectal cancer (*COAD-READ*) and lung adenocarcinoma (*LUAD*) data sets from The Cancer Genome Atlas (*TCGA*). **c** HDAC6 activity score inferred by expression of HDAC6 regulon genes upon treatment with Ricolinostat for 0, 3, 6 and 12 hours (*left*). Expression change of the HDAC6 regulon network over time upon Ricolinostat treatment at 0 and 12 hours (*right*): node is color-coded by z-score-transformed expression with *red* indicating high and *blue* low expression, and node size is also proportional to the corresponding expression. Edge is coded by the Pearson correlation of HDAC6 and corresponding regulon node with *red* indicating positive and *blue* negative, and the width is proportional to the absolute correlation value. **d** mRNA expression levels (*left*) and the HDAC6-score (*right*) in primary IBC and non-IBC clinical samples. *ARACNe* reconstruction of gene regulatory networks

unfolded protein-induced stress [18–20] (Fig. 4a). Interestingly, when we analyzed lung (TCGA LUAD)-specific and colorectal cancer (TCGA COAD-READ)-specific HDAC6 regulons, generated by ARACNe analysis of the corresponding TCGA datasets, we obtained a list of 147 and 138 genes, respectively, for which thge overlap with the breast cancer regulon was highly significant (Fig. 4b). This suggests that the transcriptional footprint of the HDAC6 regulon is highly conserved among epithelial cancer cells. Finally we integrated the expression of all transcripts in the HDAC6 regulon in a single score, termed the HDAC6 score (see “Methods”).

To demonstrate that the HDAC6 score is an indicator of the HDAC6 activity, SUM149 cells were treated for 3, 6 and 12 hours with 2.5 μ M of Ricolinostat and the HDAC6 score for treated samples was compared to controls. This study revealed that inhibition of HDAC6 significantly attenuated the HDAC6 score (Fig. 4c and Figure S3a in Additional file 5).

Finally, we evaluated the HDAC6 score in our series of 63 IBC and 134 non-IBC primary specimens. Importantly, IBCs had a significantly higher HDAC6 score than non-IBCs (Fig. 4d). To further study whether the HDAC6 score was influenced by the different composition in molecular subtypes between IBCs and non-IBCs [53] we evaluated the HDAC6 score after stratifying the tumor series based on their hormone receptor (HR) status and their intrinsic molecular subtype [54]. Our results revealed that the HDAC6 score was significantly higher in IBCs compared with non-IBC independently of those molecular characteristics (Figure S3b in Additional file 5). Furthermore, multivariate analysis taking into account these molecular classifications demonstrated that there is no significant difference between the multi-variable model, considering PAM50, ER–PR or both, and the single model with IBC only. These data show that inflammatory vs. non-inflammatory is the main feature that impacts on the HDAC6 score (see table in Additional file 1). Overall these data revealed correlation between IBC disease and the HDAC6 score, which suggests a rationale for IBC dependency on HDAC6.

Discussion

Inflammatory breast cancer is the deadliest clinical subtype of breast cancer and also one of the most poorly characterized at the molecular level. Poor understanding of this malignancy has greatly limited its therapeutic management. Our finding that IBC cells are more sensitive than non-IBC cells to HDAC6 inhibition represents a novel opportunity to develop therapeutic regimens specifically suited for IBC patients. The relevance of our data is enhanced by the fact that small molecule inhibitors for HDAC6 are

already in clinical trials (<https://clinicaltrials.gov/ct2/results?term=acy-1215&Search=Search>) and there are already maximum tolerated dose, toxicity and pharmacokinetic data from phase I studies. Consequently the transition of our finding to clinical studies can be greatly accelerated.

HDAC6 is a class-IIb histone deacetylase located mainly in the cytosol, which displays diverse functions through the deacetylation of multiple substrates [19, 55]. During the last decade, HDAC6 has emerged as a master regulator of the cellular protective response to accumulation of protein aggregates and damaged mitochondria [18–20]. Misfolded polypeptides can be corrected by chaperones [55]; however, when chaperone capacity is exceeded, they form toxic intracellular protein aggregates that are then eliminated by the proteasome and the aggresome-autophagy pathway [19, 55]. HDAC6 was discovered to be an essential component of the aggresome and HDAC6-deficient cells fail to clear misfolded proteins [18–20]. This generates endoplasmic reticulum (EnR) stress and triggers an evolutionarily conserved response termed the unfolded protein response (UPR). Initially the UPR activates pro-survival mechanisms; however, if persistent, it leads to cell death [56, 57]. Similarly, dysfunctional mitochondria aggregate into aggresome-like structures also dependent on HDAC6, called the mito-aggresome [55, 58]. Accumulation of defective mitochondria also generates toxicity that compromises cell viability [59, 60].

Why are IBC cells more dependent on HDAC6 function? Based on the current knowledge of HDAC6 function, some hypotheses appear especially reasonable (Fig. 5). It is possible that IBC cells rely on the aggresome-lysosome to clear toxic aggregates (protein, mitochondria or both) more than non-IBC cells. Dependency on HDAC6 function may be associated with higher steady-state levels of misfolded proteins and/or damaged mitochondria and saturation of alternative detox pathways such as proteasome-mediated proteolysis. Thus, in those cases blockage of HDAC6 will impact IBC homeostasis more severely. Alternatively, the differential response to HDAC6 inhibition could be determined by the stress levels already present in the cells potentially even mediated by an altered microenvironment in this disease. Homeostatic decisions in a cell, such as life or death, are the result of multiple stimuli [61, 62], and thus IBC sensitivity to HDAC6 inhibition may be determined by non-HDAC6 specific stressors already operational in the cell. Apoptotic thresholds or baseline levels of pro-apoptotic proteins may already be higher in IBC cells and may need relatively little further accumulation, such as EnR stress caused by HDAC6 inhibition, to commit themselves to apoptosis [20, 63, 64]. However, if the last was true and IBC cells were primed for apoptosis they should demonstrate sensitivity for any

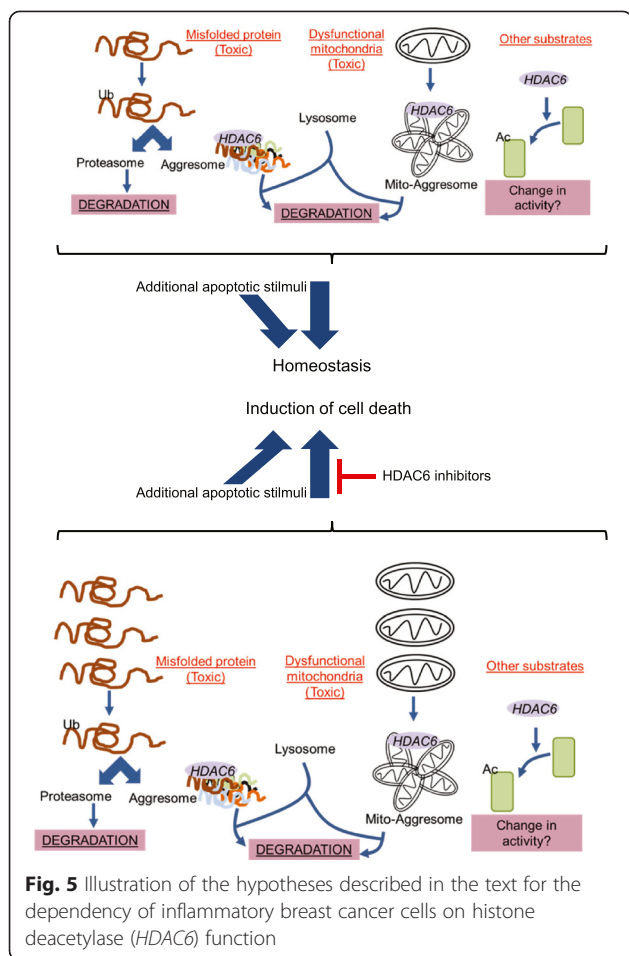


Fig. 5 Illustration of the hypotheses described in the text for the dependency of inflammatory breast cancer cells on histone deacetylase (HDAC6) function

type of additional stress. But this is not the case and we did not observe increased cell death in IBC cells compared to non-IBC when these were treated with paclitaxel (Figure S4 in Additional file 6).

Finally, we should not dismiss the importance that other HDAC6 substrates may have in the sensitivity of IBC cells to HDAC6 inhibition. For instance, the chaperone HSP90 is well-known to be a substrate of HDAC6 and consequently HDAC6 inhibition leads to hyperacetylation of HSP90 and loss of its function [65]. Remarkably, loss of HSP90 function impairs the stability of genes involved in tumorigenesis and tumor maintenance such as HIF-1 alpha [66], the breast cancer metastasis suppressor 1, BRMS1 [67] or c-Raf and AKT [68].

Some limitations of our study need to be discussed. In contrast to non-IBC cell lines, where multiple models are available representing the major molecular subtypes and origin source (primary vs. metastatic site), far fewer IBC models have been described in the literature [69]. We were unable to obtain all of these models and consequently we could only include the four that are available in our study. Although the reduced number of IBC lines can influence the functional studies presented here,

there are some facts that support a general impact of HDAC6 function on IBCs. First, half of the IBC models that were used in our studies represent the luminal subtype and the other half represent the basal subtype. As HDAC6 inhibition compromised the growth of all these IBC models a potential subtype bias is reduced. Second, the strong association between the HDAC6 score and IBC disease was found on analyzing primary tumors, which argues against a potential bias between primary and metastatic cells.

Conclusions

Overall, our data represent novel preclinical studies validating HDAC6 inhibition as an anticancer strategy for IBC patients. Two additional considerations for translating our finding to the clinical setting are worth mentioning. The first is the potential combination of HDAC6 inhibition with other therapeutic strategies. Multimodal therapy is the standard approach for the vast majority of solid tumors including breast cancers regimens based on targeted therapies [70]. Remarkably, synergistic activity between HDAC6 and proteasome inhibitors [21], and HDAC6 inhibition and taxanes [71] has been described. The second is the potential use of the HDAC6 score to identify individual tumors that may be sensitive to this new modality of targeted therapy. Preselection of patients for HDAC6 therapy using the HDAC6 score as a predictive biomarker may be applicable not only to IBCs but also to non-IBCs and other tumors. Future studies should further investigate the mechanistic basis of the sensitivity of IBC cells to HDAC6 inhibition and the predictive potential of the HDAC6 score in order to efficiently apply targeted HDAC6 therapy in IBC.

Additional files

Additional file 1: Supplementary material and methods. Includes more detailed information about the methodology of the shRNA screens and the supplementary Tables 2 and 3. (DOCX 815 kb)

Additional file 2: Figure S1. Quality control studies of the shRNA screens. **a** Representative image showing the Pearson and Spearman correlation among the triplicates for T = 10 in the SUM149 cell line. **b** GO-term and KEGG-pathway analyses using genes commonly depleted in several cell lines ($p < 0.05$ in ≥ 3 cell lines, 2,555 genes) show enrichment of genes related to essential functions. **c** Essential genes depleted in our shRNA screen cell lines overlapped significantly with compiled screens across 72 cell lines and subtypes of cancer (Fisher's exact test). (EPS 3172 kb)

Additional file 3: Table S1. List of 71 candidate genes significantly and globally depleted in inflammatory breast cancer (IBC) lines vs. non-IBC ($p < 0.05$ and \log_2 fold-change or $\log_2FC < -1$). (XLS 98 kb)

Additional file 4: Figure S2. Inhibition of HDAC6 activity by small molecules in vitro and in vivo. The western blots show the accumulation of Ac- α -tubulin when SUM149 cells were treated with Ricolinostat and Tubastatin-A in vitro (**a**) and in vivo (**b**). (EPS 783 kb)

Additional file 5: Figure S3. Changes in the HDAC6 regulon network upon Ricolinostat treatment and HDAC6 score in primary breast cancers. **a** Alternative view of expression change of HDAC6 regulon network over

time upon Ricolinostat treatment at 0 and 12 hours as shown in Fig. 4c. **b** The dot-plots show the HDAC6 scores in the inflammatory breast cancer (IBC) and non-IBC primary tumor series when these samples were stratified based on their HR status (*left*) and their PAM-50 molecular subtype (*right*). (EPS 8784 kb)

Additional file 6: Figure S4. Response to paclitaxel treatment in breast cancer cell line models. The bars indicates the normalized survival after different breast cancer cell lines (inflammatory breast cancer (IBC) and non-IBC) were treated for two doubling times with 10 uM of paclitaxel. Expression change of HDAC6 regulon network over time upon Ricolinostat treatment. (EPS 713 kb)

Abbreviations

ARACNe: reconstruction of gene regulatory networks; ATCC: American Type Culture Collection; bp: base pairs; BRCA: breast cancer; CNV: copy number variation; COAD: colorectal adenocarcinoma; DAVID: Database for Annotation, Visualization, and Integrated Discovery; DMSO: dimethyl sulfoxide; DPI: data processing inequality; ER: estrogen receptor; gDNA: genomic DNA; GEO: Gene Expression Omnibus; GO: Gene Ontology; GSEA: gene set enrichment analysis; HDAC: histone deacetylase; HER2: human epidermal growth factor receptor-2; HTP: high throughput; IBC: inflammatory breast cancer; log2FC: log2 fold-change; LUAD: lung adenocarcinoma; MARINA: master regulator inference algorithm; METABRIC: Molecular Taxonomy of Breast Cancer International Consortium; MOI: multiplicity of infection; NB: number of bootstraps; PR: progesterone receptor; shRNA: short hairpin RNA; TGCA: The Cancer Genome Atlas; UPR: unfolded protein response.

Competing interests

Steven N. Quayle and, Min Yang are employees of Acetylon Pharmaceuticals, Inc. I confirm that no other author has any competing interests in the manuscript.

Authors' contributions

PP and RR performed the experimental validation of HDAC6 as target described in the text and helped to draft the manuscript. JY performed all the computational analysis and helped to draft the manuscript. LS, PV, EM, VC and DLI performed the 15 different shRNA screens described in the text and helped to draft the manuscript. SQ and MY prepared, QC and provided all the ACY inhibitors and helped to draft the manuscript. DB, PF and FB acquired and analyzed the data related to IBC and non-IBC primary samples and helped to draft the manuscript. WW and MA generated, maintained and provided the IBC-3 and Mary-x models respectively and helped to draft the manuscript. AC and JS conceived of the study, and participated in its design and coordination and drafting of the manuscript. All authors read and approved the final manuscript.

Acknowledgements

This work was supported by the NIH grant R01/EUREKA R01CA153233 and the Breast Cancer Alliance (Jose Silva) and for the NCC (Ruth Rodriguez-Barrueco).

Author details

¹Department of Pathology, Icahn School of Medicine at Mount Sinai, New York, NY 10029-6574, USA. ²Department of Biomedical Informatics, Department of Systems Biology, Center for Computational Biology and Bioinformatics, Herbert Irving Comprehensive Cancer Center, Columbia University, New York, NY 10032, USA. ³Department of Biochemistry and Molecular Biophysics, Institute for Cancer Genetics, Columbia University, New York, NY 10032, USA. ⁴Herbert Irving Comprehensive Cancer Center, Columbia University, 1130 St. Nicholas Avenue, New York, NY 10032, USA. ⁵Department of Pathology, Columbia University Medical Center, 630 West 168th Street, New York, NY 10032, USA. ⁶Acetylon Pharmaceuticals, Inc., 70 Fargo St, Suite 205, Boston, MA 02210, USA. ⁷Department of Surgery, Memorial Sloan Kettering Cancer Center, New York, NY 10065, USA. ⁸Department of Radiation Oncology, The University of Texas MD Anderson Cancer Center, Houston, TX, USA. ⁹Centre de Recherche en Cancérologie de Marseille, Institut Paoli-Calmettes, Aix-Marseille Université, Marseille, France.

Received: 19 August 2015 Accepted: 25 November 2015

Published online: 08 December 2015

References

- Hance KW, Anderson WF, Devesa SS, Young HA, Levine PH. Trends in inflammatory breast carcinoma incidence and survival: the surveillance, epidemiology, and end results program at the National Cancer Institute. *J Natl Cancer Inst.* 2005;97(13):966–75.
- Matro JM, Li T, Cristofanilli M, Hughes ME, Ottesen RA, Weeks JC, et al. Inflammatory Breast Cancer Management in the National Comprehensive Cancer Network: The Disease, Recurrence Pattern, and Outcome. *Clin Breast Cancer.* 2014.
- van Uden DJ, van Laarhoven HW, Westenberg AH, de Wilt JH, Blanken-Peeters CF. Inflammatory breast cancer: an overview. *Crit Rev Oncol Hematol.* 2015;93(2):116–26.
- Dawood S, Ueno NT, Cristofanilli M. The medical treatment of inflammatory breast cancer. *Semin Oncol.* 2008;35(1):64–71.
- Luo J, Solimini NL, Elledge SJ. Principles of cancer therapy: oncogene and non-oncogene addiction. *Cell.* 2009;136(5):823–37.
- Weinstein IB, Joe AK. Mechanisms of disease: Oncogene addiction—a rationale for molecular targeting in cancer therapy. *Nat Clin Pract Oncol.* 2006;3(8):448–57.
- Houchens NW, Merajver SD. Molecular determinants of the inflammatory breast cancer phenotype. *Oncology (Williston Park).* 2008;22(14):1556–61. discussion 1561, 1565-1558, 1576.
- Bertucci F, Finetti P, Vermeulen P, Van Dam P, Dirix L, Birnbaum D, et al. Genomic profiling of inflammatory breast cancer: a review. *Breast.* 2014;23(5):538–45.
- Silva JM, Li MZ, Chang K, Ge W, Golding MC, Rickles RJ, et al. Second-generation shRNA libraries covering the mouse and human genomes. *Nat Genet.* 2005;37(11):1281–8.
- Paddison PJ, Silva JM, Conklin DS, Schlabach M, Li M, Aruleba S, et al. A resource for large-scale RNA-interference-based screens in mammals. *Nature.* 2004;428(6981):427–31.
- Silva JM, Ezhkova E, Silva J, Heart S, Castillo M, Campos Y, et al. Cyfip1 is a putative invasion suppressor in epithelial cancers. *Cell.* 2009;137(6):1047–61.
- Silva JM, Marran K, Parker JS, Silva J, Golding M, Schlabach MR, et al. Profiling essential genes in human mammary cells by multiplex RNAi screening. *Science.* 2008;319(5863):617–20.
- Rodriguez-Barrueco R, Marshall N, Silva JM. Pooled shRNA screenings: experimental approach. *Methods Mol Biol.* 2013;980:353–70.
- Yu J, Putcha P, Califano A, Silva JM. Pooled shRNA screenings: computational analysis. *Methods Mol Biol.* 2013;980:371–84.
- Marcotte R, Brown KR, Suarez F, Sayad A, Karamboulas K, Krzyzanowski PM, et al. Essential gene profiles in breast, pancreatic, and ovarian cancer cells. *Cancer Discov.* 2012;2(2):172–89.
- Brough R, Frankum JR, Sims D, Mackay A, Mendes-Pereira AM, Bajrami I, et al. Functional viability profiles of breast cancer. *Cancer Discov.* 2011;1(3):260–73.
- Lord CJ, McDonald S, Swift S, Turner NC, Ashworth A. A high-throughput RNA interference screen for DNA repair determinants of PARP inhibitor sensitivity. *DNA Repair (Amst).* 2008;7(12):2010–9.
- Kawaguchi Y, Kovacs JJ, McLaurin A, Vance JM, Ito A, Yao TP. The deacetylase HDAC6 regulates aggressive formation and cell viability in response to misfolded protein stress. *Cell.* 2003;115(6):727–38.
- Matthias P, Yoshida M, Khochbin S. HDAC6 a new cellular stress surveillance factor. *Cell Cycle.* 2008;7(1):7–10.
- Boyault C, Zhang Y, Fritah S, Caron C, Gilquin B, Kwon SH, et al. HDAC6 controls major cell response pathways to cytotoxic accumulation of protein aggregates. *Genes Dev.* 2007;21(17):2172–81.
- Santo L, Hideshima T, Kung AL, Tseng JC, Tamang D, Yang M, et al. Preclinical activity, pharmacodynamic, and pharmacokinetic properties of a selective HDAC6 inhibitor, ACY-1215, in combination with bortezomib in multiple myeloma. *Blood.* 2012;119(11):2579–89.
- Sims D, Mendes-Pereira AM, Frankum J, Burgess D, Cerone MA, Lombardelli C, et al. High-throughput RNA interference screening using pooled shRNA libraries and next generation sequencing. *Genome Biol.* 2011;12(10):R104.
- Basik MC, Lebbink RJ, Churchman LS, Ingolia NT, Patena W, LeProust EM, et al. Rapid creation and quantitative monitoring of high coverage shRNA libraries. *Nat Methods.* 2009;6(6):443–5.
- Fellmann C, Zuber J, McJunkin K, Chang K, Malone CD, Dickins RA, et al. Functional identification of optimized RNAi triggers using a massively parallel sensor assay. *Mol Cell.* 2011;41(6):733–46.

25. Baldi P, Long AD. A Bayesian framework for the analysis of microarray expression data: regularized t-test and statistical inferences of gene changes. *Bioinformatics*. 2001;17(6):509–19.
26. Chang CW, Cheng WC, Chen CR, Shu WY, Tsai ML, Huang CL, et al. Identification of human housekeeping genes and tissue-selective genes by microarray meta-analysis. *PLoS One*. 2011;6(7):e22859.
27. Stouffer SA, Suchman EA, DeVinney LC, Star SA, Williams RMJ. *Adjustment During Army Life*, vol. 1. Princeton: Princeton University Press; 1949.
28. da Huang W, Sherman BT, Lempicki RA. Systematic and integrative analysis of large gene lists using DAVID bioinformatics resources. *Nat Protoc*. 2009;4(1):44–57.
29. Subramanian A, Tamayo P, Mootha VK, Mukherjee S, Ebert BL, Gillette MA, et al. Gene set enrichment analysis: a knowledge-based approach for interpreting genome-wide expression profiles. *Proc Natl Acad Sci U S A*. 2005;102(43):15545–50.
30. Margolin AA, Nemenman I, Basso K, Wiggins C, Stolovitzky G, Dalla Favera R, et al. ARACNE: an algorithm for the reconstruction of gene regulatory networks in a mammalian cellular context. *BMC Bioinformatics*. 2006;7 Suppl 1:S7.
31. Cancer Genome Atlas N. Comprehensive molecular portraits of human breast tumours. *Nature*. 2012;490(7418):61–70.
32. Cancer Genome Atlas Research N. Comprehensive molecular profiling of lung adenocarcinoma. *Nature*. 2014;511(7511):543–50.
33. Cancer Genome Atlas N. Comprehensive molecular characterization of human colon and rectal cancer. *Nature*. 2012;487(7407):330–7.
34. Piovani E, Yu J, Tosello V, Herranz D, Ambesi-Impombato A, Da Silva AC, et al. Direct reversal of glucocorticoid resistance by AKT inhibition in acute lymphoblastic leukemia. *Cancer Cell*. 2013;24(6):766–76.
35. Lefebvre C, Rajbhandari P, Alvarez MJ, Bandaru P, Lim WK, Sato M, et al. A human B-cell interactome identifies MYB and FOXM1 as master regulators of proliferation in germinal centers. *Mol Syst Biol*. 2010;6:377.
36. Carro MS, Lim WK, Alvarez MJ, Bollo RJ, Zhao X, Snyder EY, et al. The transcriptional network for mesenchymal transformation of brain tumours. *Nature*. 2010;463(7279):318–25.
37. Efron B, Tibshirani R. On Testing the Significance of Sets of Genes. *Ann Appl Stat*. 2007;1(1):107–29.
38. Rodriguez-Barrueco R, Yu J, Saucedo-Cuevas LP, Olivan M, Llobet-Navas D, Putcha P, et al. Inhibition of the autocrine IL-6-JAK2-STAT3-calprotectin axis as targeted therapy for HR-/HER2+ breast cancers. *Genes Dev*. 2015;29(15):1631–48. doi: 10.1101/gad.262642.115. Epub 2015 Jul.
39. Wang T, Wei JJ, Sabatini DM, Lander ES. Genetic screens in human cells using the CRISPR-Cas9 system. *Science*. 2014;343(6166):80–4.
40. Schlabach MR, Luo J, Solimini NL, Hu G, Xu Q, Li MZ, et al. Cancer proliferation gene discovery through functional genomics. *Science*. 2008;319(5863):620–4.
41. Scholl C, Frohling S, Dunn IF, Schinzel AC, Barbie DA, Kim SY, et al. Synthetic lethal interaction between oncogenic KRAS dependency and STK33 suppression in human cancer cells. *Cell*. 2009;137(5):821–34.
42. Neve RM, Chin K, Fridlyand J, Yeh J, Baehner FL, Fevr T, et al. A collection of breast cancer cell lines for the study of functionally distinct cancer subtypes. *Cancer Cell*. 2006;10(6):515–27.
43. Luo B, Cheung HW, Subramanian A, Sharifnia T, Okamoto M, Yang X, et al. Highly parallel identification of essential genes in cancer cells. *Proc Natl Acad Sci U S A*. 2008;105(51):20380–5.
44. Hubbert C, Guardiola A, Shao R, Kawaguchi Y, Ito A, Nixon A, et al. HDAC6 is a microtubule-associated deacetylase. *Nature*. 2002;417(6887):455–8.
45. De Vreese R, Verhaeghe T, Desmet T, D'Hooghe M. Potent and selective HDAC6 inhibitory activity of N-(4-hydroxycarbamoylbenzyl)-1,2,4,9-tetrahydro-3-thia-9-azafluorenes as novel sulfur analogues of Tubastatin A. *Chem Commun*. 2013;49(36):3775–7.
46. Klopp AH, Lacerda L, Gupta A, Debeb BG, Solley T, Li L, et al. Mesenchymal stem cells promote mammosphere formation and decrease E-cadherin in normal and malignant breast cells. *PLoS One*. 2010;5(8):e12180.
47. Alpaugh ML, Tomlinson JS, Shao ZM, Barsky SH. A novel human xenograft model of inflammatory breast cancer. *Cancer Res*. 1999;59(20):5079–84.
48. Xiao Y, Ye Y, Yearsley K, Jones S, Barsky SH. The lymphovascular embolus of inflammatory breast cancer expresses a stem cell-like phenotype. *Am J Pathol*. 2008;173(2):561–74.
49. Bekhouche I, Finetti P, Adelaide J, Ferrari A, Tarpin C, Charafe-Jauffret E, et al. High-resolution comparative genomic hybridization of inflammatory breast cancer and identification of candidate genes. *PLoS One*. 2011;6(2):e16950.
50. Basso K, Margolin AA, Stolovitzky G, Klein U, Dalla-Favera R, Califano A. Reverse engineering of regulatory networks in human B cells. *Nat Genet*. 2005;37(4):382–90.
51. Aytes A, Mitrofanova A, Lefebvre C, Alvarez MJ, Castillo-Martin M, Zheng T, et al. Cross-species regulatory network analysis identifies a synergistic interaction between FOXM1 and CENPF that drives prostate cancer malignancy. *Cancer Cell*. 2014;25(5):638–51.
52. Lefebvre C, Rieckhof G, Califano A. Reverse-engineering human regulatory networks. *Wiley Interdiscip Rev Syst Biol Med*. 2012;4(4):311–25.
53. Bertucci F, Finetti P, Rougemont J, Charafe-Jauffret E, Cervera N, Tarpin C, et al. Gene expression profiling identifies molecular subtypes of inflammatory breast cancer. *Cancer Res*. 2005;65(6):2170–8.
54. Perou CM, Sorlie T, Eisen MB, van de Rijn M, Jeffrey SS, Rees CA, et al. Molecular portraits of human breast tumours. *Nature*. 2000;406(6797):747–52.
55. Yan J. Interplay between HDAC6 and its interacting partners: essential roles in the aggresome-autophagy pathway and neurodegenerative diseases. *DNA Cell Biol*. 2014;33(9):567–80.
56. Ron D, Walter P. Signal integration in the endoplasmic reticulum unfolded protein response. *Nat Rev Mol Cell Biol*. 2007;8(7):519–29.
57. Xu C, Bailly-Maitre B, Reed JC. Endoplasmic reticulum stress: cell life and death decisions. *J Clin Invest*. 2005;115(10):2656–64.
58. Lee JY, Nagano Y, Taylor JP, Lim KL, Yao TP. Disease-causing mutations in parkin impair mitochondrial ubiquitination, aggregation, and HDAC6-dependent mitophagy. *J Cell Biol*. 2010;189(4):671–9.
59. Hu F, Liu F. Mitochondrial stress: a bridge between mitochondrial dysfunction and metabolic diseases? *Cell Signal*. 2011;23(10):1528–33.
60. Shokolenko I, Venediktova N, Bochkareva A, Wilson GL, Alexeyev MF. Oxidative stress induces degradation of mitochondrial DNA. *Nucleic Acids Res*. 2009;37(8):2539–48.
61. Evan GI, Vousden KH. Proliferation, cell cycle and apoptosis in cancer. *Nature*. 2001;411(6835):342–8.
62. Danial NN, Korsmeyer SJ. Cell death: critical control points. *Cell*. 2004;116(2):205–19.
63. Chen S, Zhang Y, Zhou L, Leng Y, Lin H, Kmiecik M, et al. A Bim-targeting strategy overcomes adaptive bortezomib resistance in myeloma through a novel link between autophagy and apoptosis. *Blood*. 2014;124(17):2687–97.
64. Hideshima T, Richardson PG, Anderson KC. Mechanism of action of proteasome inhibitors and deacetylase inhibitors and the biological basis of synergy in multiple myeloma. *Mol Cancer Ther*. 2011;10(11):2034–42.
65. Kekatpure VD, Dannenberg AJ, Subbaramaiah K. HDAC6 modulates Hsp90 chaperone activity and regulates activation of aryl hydrocarbon receptor signaling. *J Biol Chem*. 2009;284(12):7436–45.
66. Qian DZ, Kachhap SK, Collis SJ, Verheul HM, Carducci MA, Atadja P, et al. Class II histone deacetylases are associated with VHL-independent regulation of hypoxia-inducible factor 1 alpha. *Cancer Res*. 2006;66(17):8814–21.
67. Hurst DR, Mehta A, Moore BP, Phadke PA, Meehan WJ, Accavitti MA, et al. Breast cancer metastasis suppressor 1 (BRMS1) is stabilized by the Hsp90 chaperone. *Biochem Biophys Res Commun*. 2006;348(4):1429–35.
68. Bali P, Pranpat M, Bradner J, Balasis M, Fiskus W, Guo F, et al. Inhibition of histone deacetylase 6 acetylates and disrupts the chaperone function of heat shock protein 90: a novel basis for antileukemia activity of histone deacetylase inhibitors. *J Biol Chem*. 2005;280(29):26729–34.
69. Fernandez SV, Robertson FM, Pei J, Aburto-Chumpitaz L, Mu Z, Chu K, et al. Inflammatory breast cancer (IBC): clues for targeted therapies. *Breast Cancer Res Treat*. 2013;140(1):23–33.
70. Tinoco G, Warsch S, Gluck S, Avancha K, Montero AJ. Treating breast cancer in the 21st century: emerging biological therapies. *J Cancer*. 2013;4(2):117–32.
71. Marcus AI, Zhou J, O'Brate A, Hamel E, Wong J, Nivens M, et al. The synergistic combination of the farnesyl transferase inhibitor lonafarnib and paclitaxel enhances tubulin acetylation and requires a functional tubulin deacetylase. *Cancer Res*. 2005;65(9):3883–93.